Asymmetric Coordination of Metal-Organic Frameworks with Enhanced Metal-Oxygen Hybridization for Li-O_2 Batteries

Bo Wen[a†], Jiaxuan An[a†], Zikang Chen[a], Yaohui Huang[a], Lutong Shan[c], Hengyi Fang[d], Ke Liu[b], Zhao Zhao[b], Zhuoliang Jiang[b*] & Fujun Li[a*]

a. Academy for Advanced Interdisciplinary Studies, Frontiers Science Center for New Organic Matter, Key Laboratory of Advanced Energy Materials Chemistry. (Ministry of Education), College of Chemistry, Nankai University, Tianjin 300071, China.

b. State Key Laboratory of Tropic Ocean Engineering Materials and Materials Evaluation, Hainan Provincial Key Lab of Fine Chem, School of Marine Technology and Equipment, Hainan University, Haikou, 570228, China.

c. Department of Chemical and Biomolecular Engineering, National University of Singapore, 117585, Singapore.

d. Jinan Key Laboratory of Advanced Energy Storage and Hydrogen Utilization, Qilu University of Technology (Shandong Academy of Sciences), Jinan 250014, PR China

† These authors contributed equally to this work.

E-mail: jiangzl@hainanu.edu.cn, fujunli@nankai.edu.cn

Experimental Sections

Synthesis of Ni-N_2S_2: 20 mM $Ni(NO_3)_2 \cdot 6H_2O$ was first dissolved in 70 mL of deionized water under stirring to form a homogeneous solution. The Ni seed layer was electrodeposited on carbon cloth (CC, 1.5 × 2.5 cm^2) substrate in the solution via galvanostatic method at -20 mA for 1200 s. Then, 0.1 mmol 2,5-diaminobenzene-1,4-dithiol dihydrochloride (DABDT) was dissolved in a mixed solution of 11.1 mL of N, N-dimethylformamide and 0.9 mL of deionized water. The mixed solution was strongly stirred for 30 min with adding 200 μL of ammonia solution. It was further transferred into a Teflon-lined autoclave (15 mL) with adding the electrodeposited CC and heated in an oven maintained at 120 ℃ for 12 h. After cooling, Ni-N_2S_2 was obtained by cleaning the substrate by ethanol and drying at 80 ℃ for 12 h in a vacuum oven.

Synthesis of Ni-N_4: Ni-N_4 was synthesized through similar processes by using 1,2,4,5-benzenetetramine tetrahydrochloride organic ligand.

Characterizations

Morphology and microstructure images were carried out by scanning electron microscopy (SEM, JEOL JSM-7900F, AEMC) and transmission electron microscopy (TEM, FEI Talos F200X G2, AEMC). XRD patterns were obtained on Rigaku Smart Lab equipped with a Cu Kα radiation source. X-ray absorption spectroscopy (XAS) measurements were measured at the P64 beamline of PETRA-III, Germany. The Ni *K*-edge (8333 eV) was collected in both transmission mode. Simultaneously, the reference spectra for energy correction were also collected by testing the corresponding transition-Ni foil. XPS spectra were detected by Thermo Fisher Scientific Escalab 250Xi. FTIR spectra were acquired in the attenuated total refection (ATR) mode on a Bruker TENSOR Ⅱ spectrometer. O_2-temperature-programmed desorption spectra (O_2-TPD) measurement were obtained on AutoChem1 Ⅱ2920 with heating rate of 10 °C min^{-1}. The UV-vis absorption spectra were collected on a Thermo Scientific Evolution 220 UV-vis spectrophotometer.

First principles calculations

All calculations in this study were performed with the Vienna ab initio Simulation Package (VASP)[1] within the frame of density functional theory (DFT). The exchange-correlation interactions of electron were described via the generalized gradient approximation (GGA) with PBE functional[2],

and the projector augmented wave (PAW) method[3] was used to describe the interactions of electron and ion. Additionally, the DFT-D3 method[4-5] was used to account for the long-range van der Waals forces present within the system. The Monkhorst-Pack scheme[6] was used for the integration in the irreducible Brillouin zone. The kinetic energy cut-off of 450 eV was chosen for the plane wave expansion. The lattice parameters and ionic position were fully relaxed, and the total energy was converged within 10^{-5} eV per formula unit. The final forces on all ions are less than 0.02 $Å^{-1}$.

Electrochemical measurements

The MOFs electrodes were cut into pieces of 1 cm in diameter as cathodes. Li-O_2 batteries (CR2032) were assembled in an Ar-filled glove box with O_2 < 0.1 ppm and H_2O < 0.1 ppm, which contains MOFs cathode, lithium metal as anode, 1 M bistrifluoromethanesulfonimide lithium (LiTFSI) in tetraethylene glycol dimethyl ether (G4) as electrolyte, and glass fiber filter as separator. All batteries were rested for 6 h in pure O_2. The electrochemical performance of Li-O_2 batteries was measured on a land CT2001A testing system. The CV measurements were carried out on a Solartron 1470E with a voltage range of 2.0-4.0 V at scan rate of 0.1 mV s^{-1}. EIS was obtained on Solartron 1470E with the frequency ranging from 10 kHZ to 0.1 HZ.

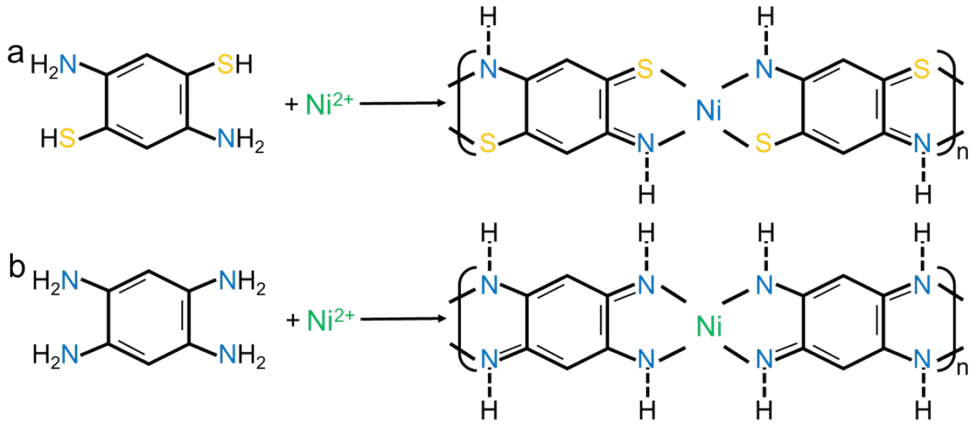

Figure S1. The coordination processes of a) Ni-N_2S_2 and b) Ni-N_4.

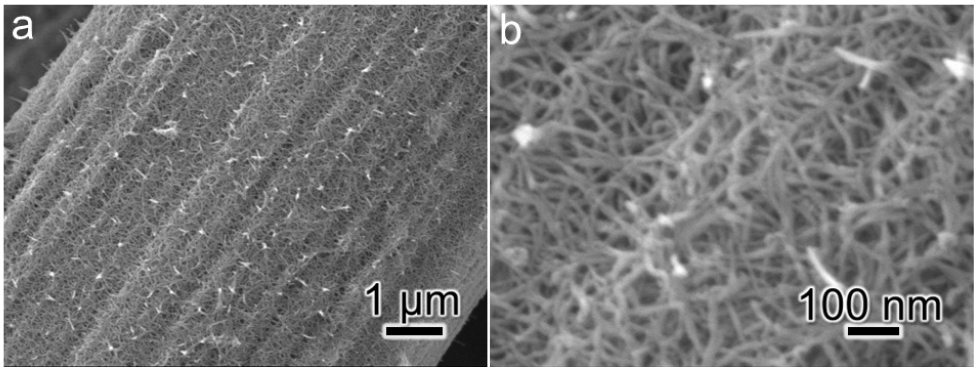

Figure S2. SEM images of Ni-N_4.

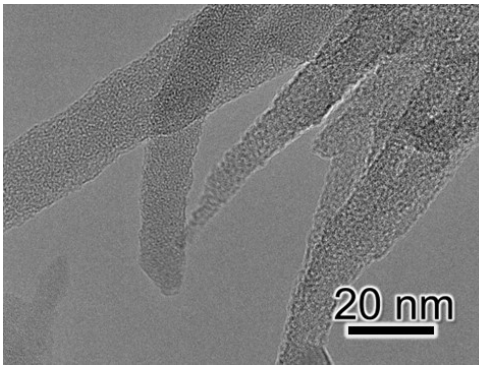

Figure S3. TEM image of Ni-N_4.

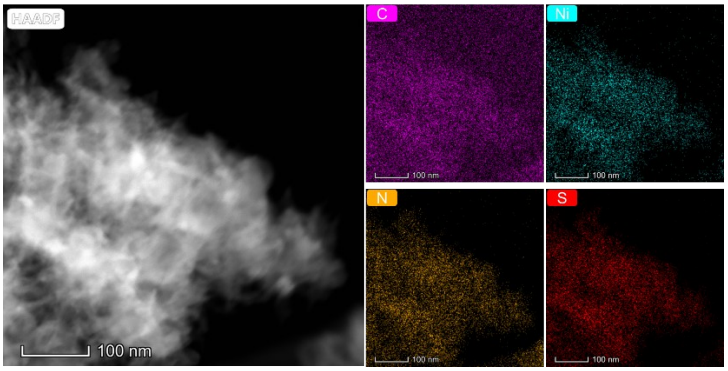

Figure S4. HAADF image and corresponding element mapping of Ni-N_2S_2.

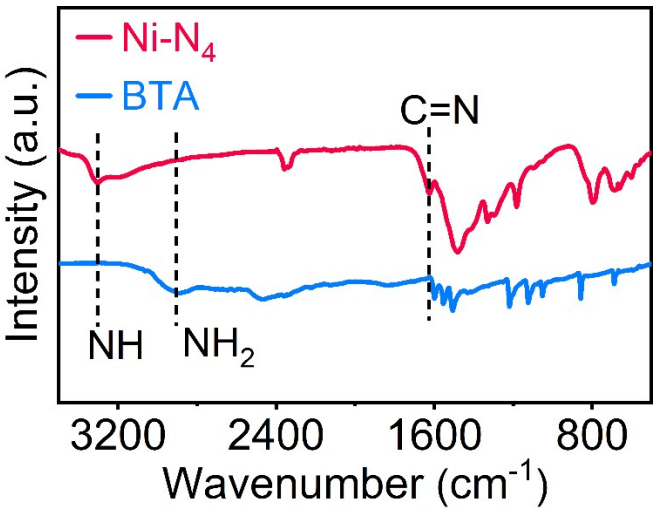

Figure S5. FTIR spectra of Ni-N_4 and BTA.

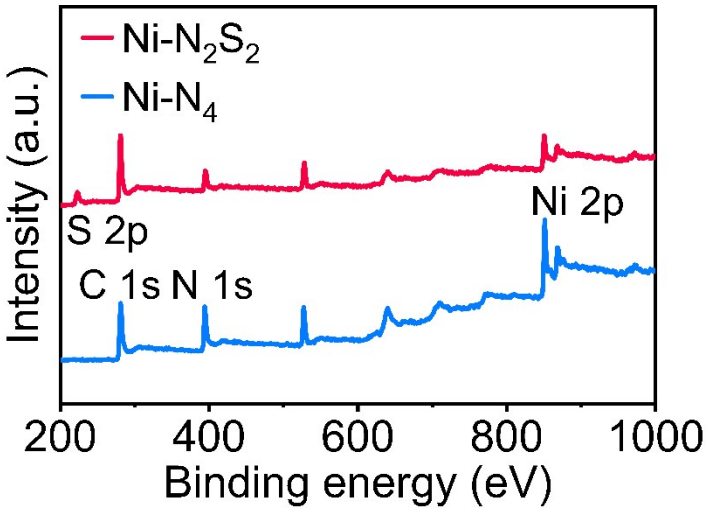

Figure S6. XPS spectra of Ni-N_2S_2 and Ni-N_4.

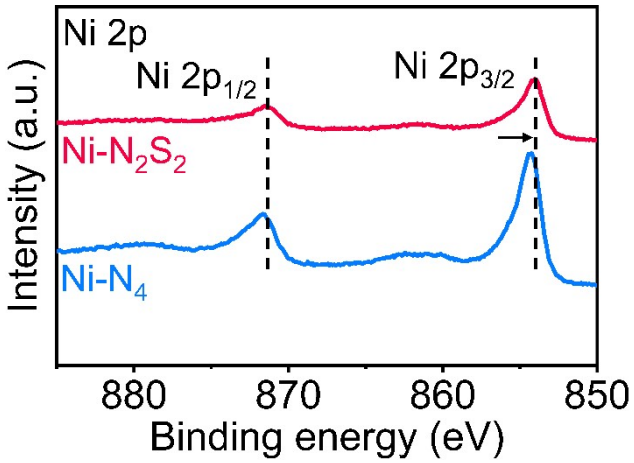

Figure S7. High-resolution Ni 2p XPS spectra of Ni-N_2S_2 and Ni-N_4.

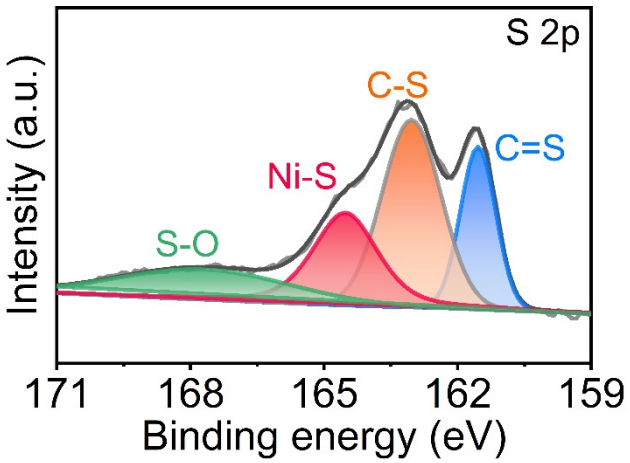

Figure S8. High-resolution S 2p XPS spectra of Ni-N_2S_2.

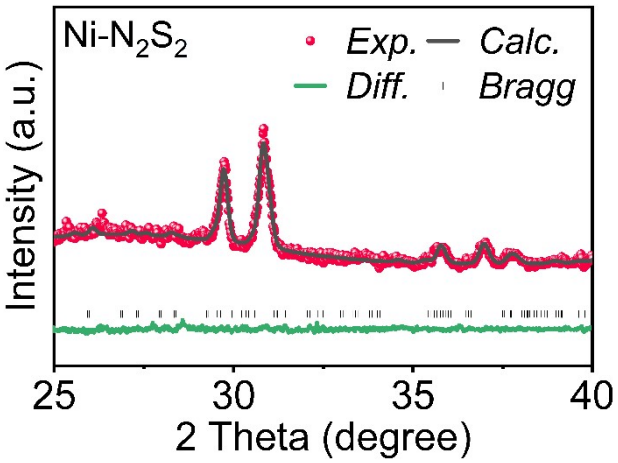

Figure S9. XRD pattern of Ni-N_2S_2.

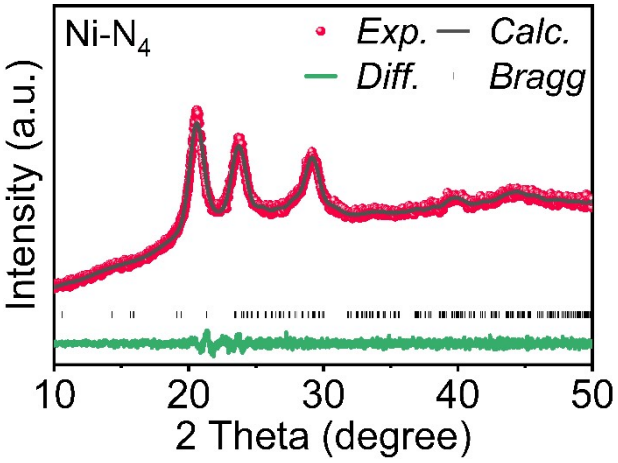

Figure S10. XRD pattern of Ni-N_4.

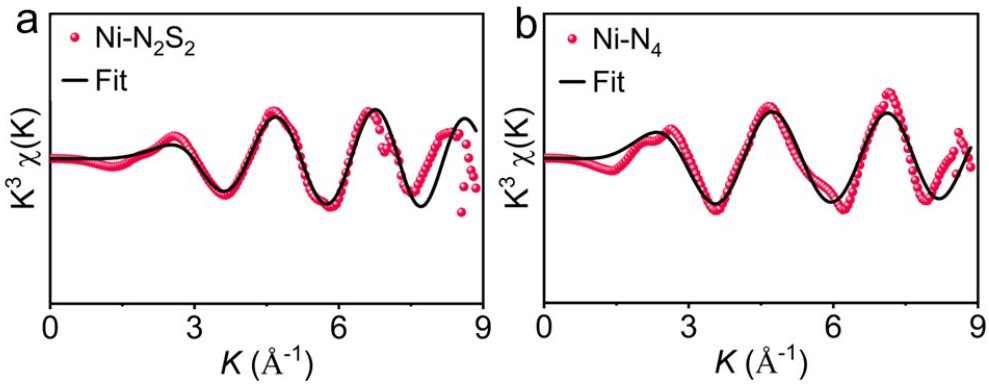

Figure S11. EXAFS fitting of a) Ni-N_2S_2 and b) Ni-N_4.

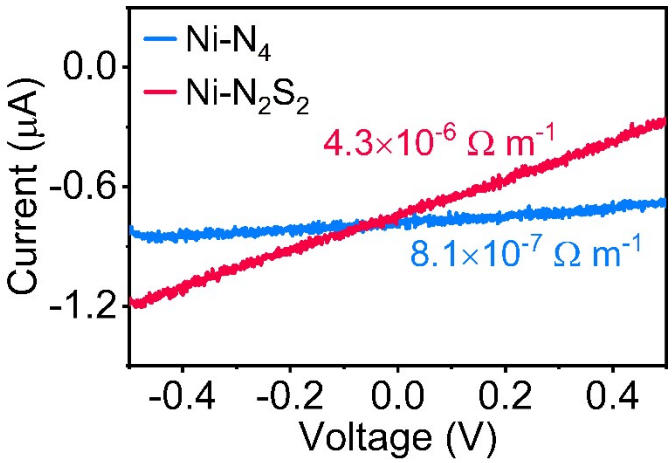

Figure S12. I-V curves of Ni-N_2S_2 and Ni-N_4.

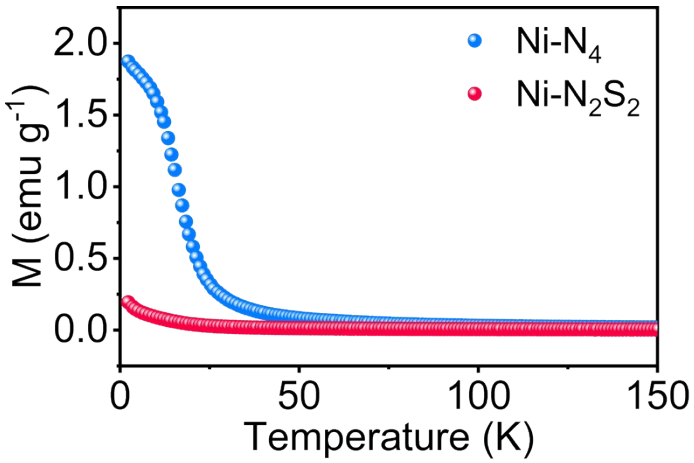

Figure S13. Temperature magnetic susceptibility of Ni-N_2S_2 and Ni-N_4.

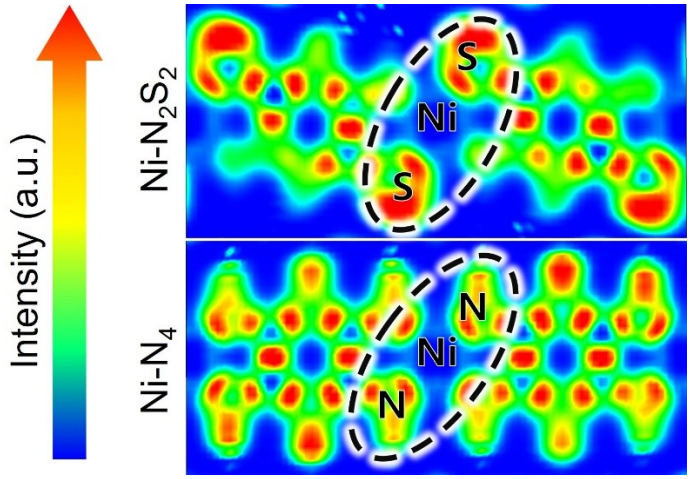

Figure S14. Electron location function of Ni-N_2S_2 and Ni-N_4.

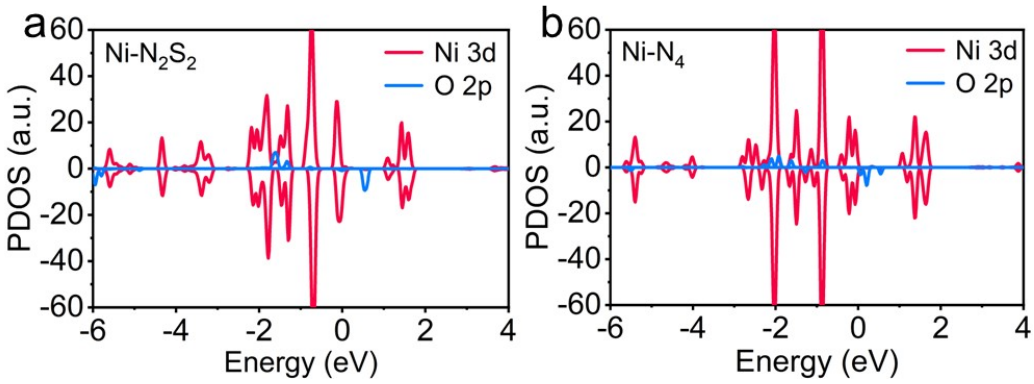

Figure S15. Density of states of Ni 3d and O 2p orbitals of a) Ni-N_2S_2 and b) Ni-N_4.

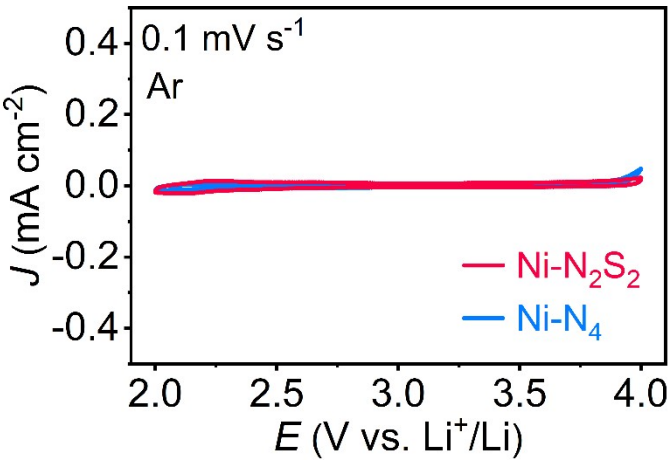

Figure S16. CV curves of Ni-N_2S_2 and Ni-N_4 based Li-O_2 batteries in Ar.

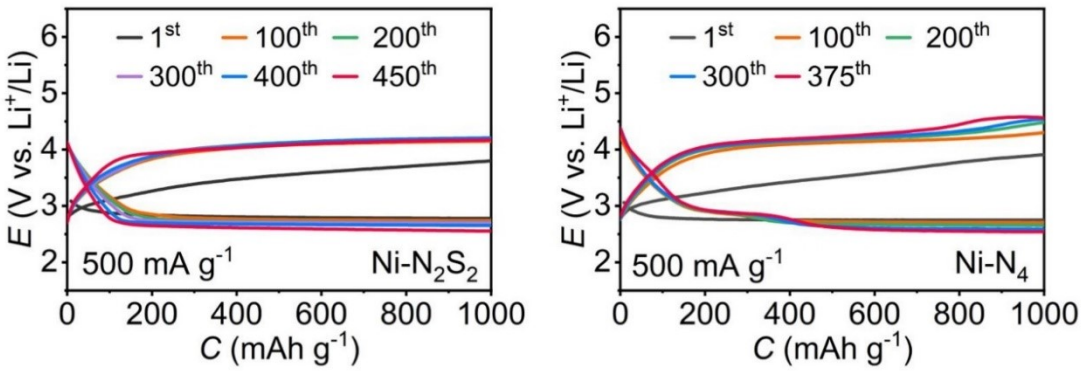

Figure S17. The discharge-charge profiles of a) Ni-N_2S_2 and b) Ni-N_4 electrodes at different cycles.

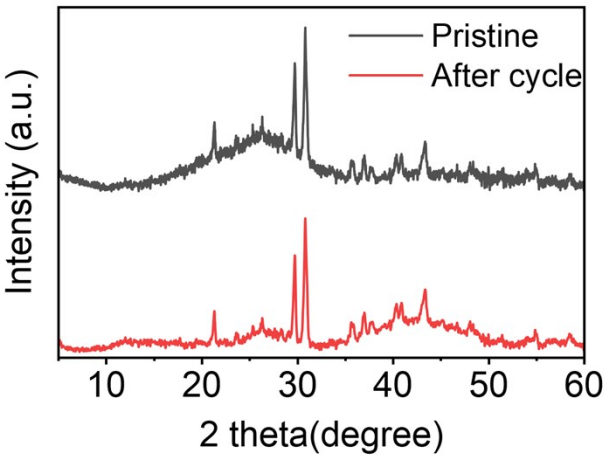

Figure S18. XRD patterns of the Ni-N_2S_2 cathode in the pristine state and after 50 cycles.

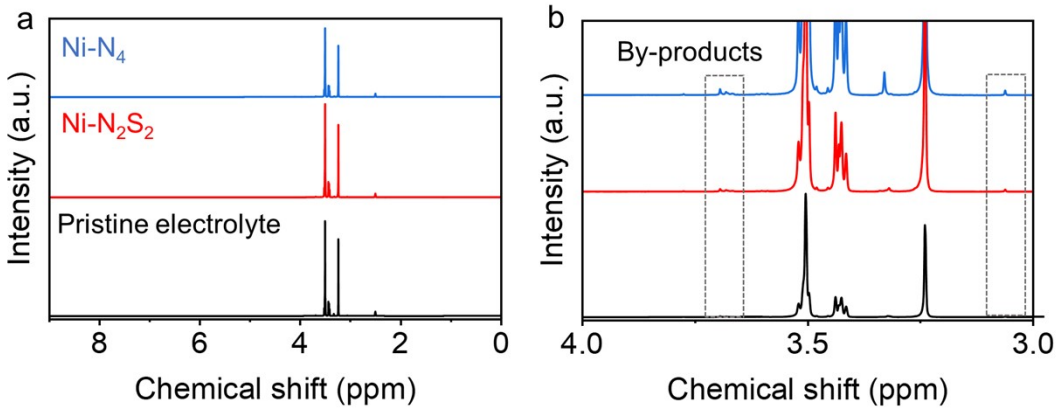

Figure S19. (a) ^{1}H NMR spectra (DMSO-d_6) of electrolytes in the pristine state and after 50 cycles. (b) Signals magnified by 200 times.

After 50 cycles, the separators from the Ni-N_4 and Ni-N_2S_2 based Li-O_2 batteries were collected and the electrolytes were extracted in deuterated DMSO-d_6 for ^{1}H-NMR analysis. The Ni-N_4 system exhibits much stronger ^{1}H-NMR signals associated with electrolyte decomposition products. This indicates that Ni-N_2S_2 can effectively suppress the decomposition of electrolytes induced by reactive oxygen species.

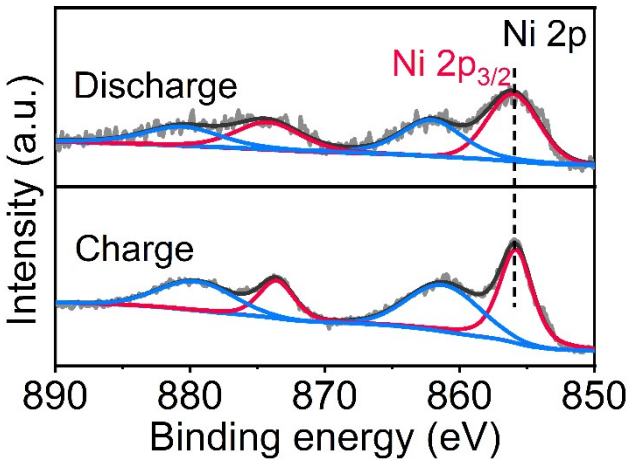

Figure S20. Ni 2p XPS of Ni-N_2S_2 electrode after discharge and recharge.

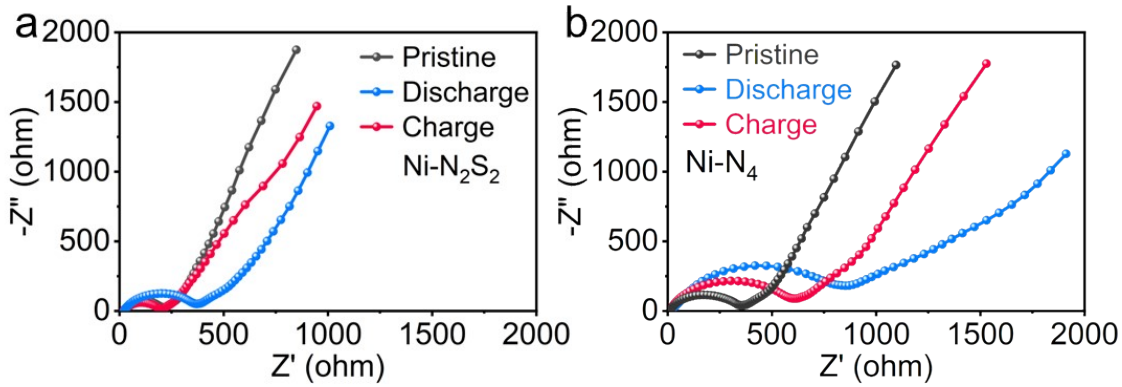

Figure 21. EIS of a) Ni-N_2S_2 and b) Ni-N_4 after discharge and charge.

Figure 22. Digital image of pouch cell with parameters.

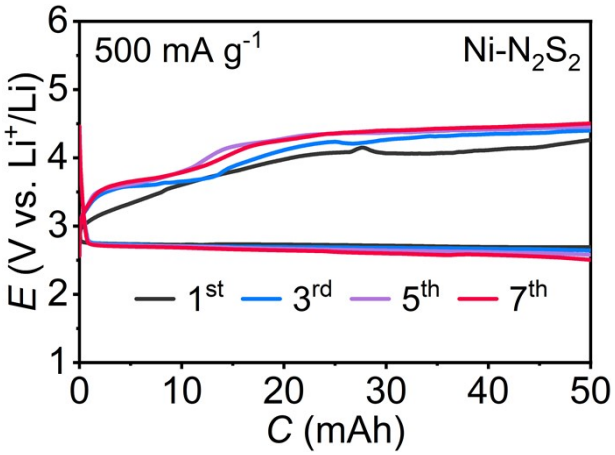

Figure 23. Discharge-charge profiles of pouch cell with Ni-N_2S_2 electrode.

Table S1. Fitted parameters of the Ni K-edge EXAFS curves of Ni-N_2S_2 and Ni-N_4.

Sample	Path	N	R (Å)	R-factor
Ni-N_2S_2	Ni-S	2	2.11±0.01	0.0086
	Ni-N	2	1.84±0.01	
Ni-N_4	Ni-N	4	1.82±0.01	0.0073

Table S2. Cyclic performances of this work and reported RuO_2-based Li-O_2 batteries.

Catalysts	Current density	Specific capacity	Cycle number	References
RuO_2 + TPA	500 mA g^{-1}	1000 mAh g^{-1}	320	7
RuO_2@polypyrrole	500 mA g^{-1}	1000 mAh g^{-1}	55	8
RuO_2@$CuFe_2O_4$	100 mA g^{-1}	1000 mAh g^{-1}	10	9
CeO_x/Ru@RuO_2	100 mA g^{-1}	1000 mAh g^{-1}	80	10
RuO_2@CoNiFe LDH	50 mA g^{-1}	500 mAh g^{-1}	50	11
Core-shell RuO_2@CNT	100 mA g^{-1}	500 mAh g^{-1}	100	12
RuO_2-Co_3O_4 nanohybrid	200 mA g^{-1}	500 mAh g^{-1}	100	13
Porous RuO_2	100 mA g^{-1}	400 mAh g^{-1}	70	14
RuO_2@N, S-codoped carbon	100 mA g^{-1}	600 mAh g^{-1}	306	15
Ni-N_2S_2	500 mA g^{-1}	1000 mAh g^{-1}	450	This work

References

1. Kresse, G.; Furthmuller, J.Efficient Iterative Schemes for Ab Initio Total-Energy calculations Using a Plane-Wave Basis Set. *Phys. Rev. B.* **1996**, 54, 11169-11186
2. Perdew, J. P., Burke, K. & Ernzerhof, M. Generalized gradient approximation made simple. *Phys. Rev. Lett*. **1996**, 77, 3865-3868.
3. Kresse, G.; Joubert, J. From Ultrasoft Pseudopotentials to the Projector Augmented-Wave Method. *Phys. Rev. B*. **1999**, 59, 1758-1775.
4. Grimme, S.; Antony, J.; Ehrlich, S.; Krieg, H. A consistent and accurate ab initio parametrization of density functional dispersion correction (DFT-D) for the 94 elements H-Pu. *J. Chem. Phys.* **2010**, *132*.
5. Grimme, S.; Ehrlich, S.; Goerigk, L. Effect of the damping function in dispersion corrected density functional theory. *J Comput Chem* **2011**, *32*, 1456-1465.
6. Monkhorst, H. J.; Pack, J. D., Special points for Brillouin-zone integrations. *Phys. Rev. B.* **1976**, 13, 5188-5192.
7. Jiang, Z.; Huang, Y.; Zhu, Z.; Gao, S.; Lv, Q.; Li, F., Quenching singlet oxygen via intersystem crossing for a stable Li-O_2 battery. Proc. Natl. Acad. Sci. USA **2022**, *119*, e2202835119.
8. Zhang, R. H.; Zhao, T. S.; Tan, P.; Wu, M. C.; Jiang, H. R., Ruthenium dioxide-decorated carbonized tubular polypyrrole as a bifunctional catalyst for non-aqueous lithium-oxygen batteries. Electrochim. Acta **2017**, *257*, 281-289.
9. Pamangadan, S. C.; Elumalai, Perumal., Enhancement of catalytic centres by RuO_2 addition to CuFe2O4 cathode catalyst for rechargeable lithium-air batteries: influence of CO_2 on Li-O_2 battery performances. Sustainable Energy Fuels, **2024**, *8*, 5581-5594.
10. Wu, X.; Zhang, Y.; Chen, S.; Zhan, X.; Zhang, H.; Zhang, Lei.; Su, L.; Shen, C.; Chen, H.; Wu, Hao.; Wang, L., Low-carbon CeOx/Ru@RuO_2 nanosheets as bifunctional catalysts for lithium-oxygen batteries. J. Alloy. Compd. **2022**, *924(30)*, 166354.
11. Lu, X.; Sakai, N.; Tang, D.; Li, X.; Taniguchi, T.; Ma, R.; Sasaki, Takayoshi., CoNiFe layered double hydroxide/RuO_2.1 nanosheet superlattice as carbon-free electrocatalysts for water splitting and Li-O_2 batteries. ACS Appl. Mater. Interfaces **2020**, *12*, 33083-33093.
12. Jian, Z.; Liu, P.; Li, F.; He, P.; Guo, X.; Chen, M.; Zhou, H., Core-shell-structured CNT@RuO_2 composite as a high-performance cathode catalyst for rechargeable Li-O_2 batteries. Angew.

Chem. Int. Ed. **2014**, *53(2)*, 442-446.

13. Zhang, Yu.; Zhang, S.; Ma, J.; Huang, A.; Yuan, M.; Li, Y.; Sun, G.; Chen, C.; Nan, C., Oxygen vacancy-rich RuO_2-Co_3O_4 nanohybrids as improved electrocatalysts for Li-O_2 batteries. ACS Appl. Mater. Interfaces 2021, 13(33), 39239-39247.
14. Zheng, M.; Jiang, J.; Lin, Z.; He, P.; Shi, Y.; Zhou H., Stable voltage cutoff cycle cathode with tunable and ordered porous structure for Li-O_2 batteries. Small **2018**, *14(47)*, 1803607.
15. Li, J.; Huang, L.; Duan, D.; Li, X.; Song, H.; Liao S., Biogelatin-derived and N,S-codoped 3D network carbon materials anchored with RuO_2 as an efficient cathode for rechargeable Li-O_2 batteries. J. Phys. Chem. C **2021**, *125(40)*, 21914-21921.